Numerical study of slip and Magnetohydrodynamics (MHD) in calendering process using non-Newtonian fluid

[a]M. A. Javed, [a]U. Shehzadi, [b]Ahmed S. Sowayan , [c]H. M. Atif, [d*]Mubbashar Nazeer, [e]Sami Ullah Khan

[a] Department of Mathematics, The University of Lahore, Gujrat campus 50700**,** Pakistan

[b]Mechanical Engineering, College of Engineering, Al Imam Mohammad Ibn Saud Islamic University (IMSIU) Riyadh, Saudi Arabia.

[c]Department of Mathematics, University of Sialkot, Pakistan

[d]Department of Mathematics, Institute of Arts and Sciences, Government College University, Faisalabad, Chiniot Campus 35400, Pakistan

[e]Department of Mathematics, Namal University, Mianwali 42250, Pakistan

*Corresponding author email: (mubbasharnazeer@gcuf.edu.pk)

Abstract

In this study, calendering process of an Oldroyd 4-constant model with the non-linear slip condition is presented. The fundamental laws are used to formulate the flow equations and then are simplified under lubrication approximation theory. We introduced the stream function to eradicate the pressure gradient and then numerically solved the final equations using the "bvp4c method" to determine the stream function and velocity profiles. The pressure gradient, pressure, and mechanical quantities of calendering operations are computed using the Runge-Kutta 4th-order approach. Using a variety of graphs, it is discussed how the slip, Hartmann number, and material parameters of an Oldroyd 4-constant fluid affect the velocity, pressure gradient, and other associated characteristics of calendering. The results reveal that on comparing to the no-slip situation, the pressure distribution inside the calender and the length of contact decreases with increasing slip parameter values. On the other hand, the Hartmann number is responsible to enhance pressure. Furthermore, a reduction is observed in final sheet thickness with increases the values of the slip parameter (Kn). The force and power are the decreasing function of α_1, conversely, these quantities increase with enhancing the values of leave off distance (λ).

Keywords: Viscoelastic fluid; Calendering; Slip condition; Hartmann number; Lubrication Approximation theory.

1. Introduction

Calendering of molten polymers is a squeezing technique that employs two anti-clockwise revolving rolls to produce a continuous sheet or film with uniform thickness. Calendering mechanisms are widely used in many industries for finishing the layout of various shapes and thicknesses of paper, fabric, or plastic film. More than 90 years ago, an abstract calendering technique was developed. The first natural rubber processing was carried out in the 1830s by two American scientists named Edwin Chaffee and Charles Goodyear, who used only two roll mills. Ardichvili [1] did, however, conduct the first quantitative research on calendering. He investigated the flow problem with the Newtonian hydrodynamics model and the lubrication approximation theory (LAT). Gaskell made the first hydrodynamic model of calendering [2]. He conducted experiments using Newtonian and Bingham fluid to study the calendering analysis. His assumptions were based on the premise of minimal roll curvature. The experimental pressure distribution measurement carried out by Bergen and Scott [3] provided support for the viability of his hypothesis. The use of pressure distribution by Bergen and Scott allowed Gaskell's theoretical results and his model to be empirically confirmed. A hyperbolic tangent model was studied by Alston and Astill [4] and Brazinsky et al. [5] examined the power-law fluid in calendering. For the Weissenberg number of less than one, Paslay [6] was able to arrive at an approximate solution that was mostly based on the Maxwell fluid. According to the outcomes of his numerical solution, when the elastic shear modulus was decreased, the shear stress and the pressure also decreased. The issues with asymmetric rolls, roll speeds, and fluid flow and heat transfer systems have received a lot of attention but have not made much headway until lately. The bipolar cylindrical coordinates were used by Takserman-Krozer, et al.[7] to investigate the asymmetrical calendering problem. The finite element approach was used by Kiparissides and Vlachopoulous[8] to investigate the power-law fluid's influence on viscous dissipation in the symmetric calendering mechanism. Chong [9] examined the hydrodynamic theory of calendering for three constitutive equations namely; the Oldroyd-B equation, the power-law equation, and a modified second-order equation; however the velocity profile cannot be obtained analytically. Mckelvey [10] carried out extensive study on calendering techniques utilizing exclusively viscous power-law fluids. Furthermore, Middleman [11] and Tadmor and Gogos [12] provided thorough theoretical insights into calendering in their respective polymer processing

publications. Dobbles and Mewis [13] conducted no-isothermal study on the calendering with temperature dependent properties.

A 3D calendering study by utilizing Newtonian fluids was conducted by Luther and Mewis [14]. They solved the problem numerically using finite element method. Sofou and Mitsoulis [15] published numerical data on the viscoplastic calendering of sheets of finite thickness. Mitsoulis and Sofou [16] also addressed the slip effects that occur on the surface of calendar rolls. Theoretical analysis of calendering concerning an incompressible Newtonian fluid with pressure-dependent viscosity was carried out by Hernandez et al. [17]. They used the perturbation method and renowned lubrication approximation theory. Arcos et al. [18] investigated the effect of non-isothermal circumstances on calendering with a viscoplastic fluid. Levine et al. [19] detailed analysis of the two-dimensional flow of a calendering device including a power-law fluid presented. To simplify the governing equations, lubrication approximation theory was employed. The final version of the flow equations is computed using the numerical finite element approach.

Ali et al. [20, 21] studied the final sheet thickness and other related quantities of calendering using different non-Newtonian fluid models. Sajid et al. [22, 23] investigate the flow in the process o calendering using third order and Rabinowitsch fluid models. Javed et al. [24-30] conducted considerable study on the calendering mechanism using different fluid models, employing both analytical and numerical methods to tackle the problem. Atif et al [31] investigated the calendering processes using Oldroyd 4-constant model. Zaheer and Khaliq [32] and whereas Zaheer et al. [33, 34] employed non-isothermal study of the calendering analysis using a water-copper nanofluid, Sutterby and Prandtl fluid models.

In these articles [35-39] different researcher demonstrated the detailed analysis of non-Newtonian fluid problems using different numerical and analytical methods and various configurations. The effects of the MHD with heat transfer analysis using different non-Newtonian fluid models in different configuration are discussed by Hsiao in the following articles[40-43]. Similarly, magnetohydrodynamic (MHD) fluid flow in the microchannel was discussed Ragueb et al. [44]. Ragueb and Mansouri [45] find the exact solution of the Greatz problem in elliptical duct using Generalized Integral Transform Method. Nazeer et al. [46-50] is also highlighted the applications of non-Newtonian fluids through different configurations.

No attempt is available where the Hartmann number and slip effects are studied using non-Newtonian fluid. Therefore, the basic objective of this study is to explore the numerical

solution of the calendering of MHD non-Newtonian fluid with slip effects on the velocity of the molten polymer sheet, pressure, power function, and final sheet thickness. The structure of the current study is as follows. Section 1 described the literature survey, section 2 provides problem statement and formulation, section 3 consist resolution method. Section 4 presents numerical findings and discussions. In Section 5, there is a succinct summary.

2. Problem Statement and Formulation

In order to study the MHD and slip effects in the calendering process, we used the basic equations of continuity and momentum for incompressible fluids are defined as: *aa*

$$div\mathbf{V}^* = 0, \tag{1}$$

$$\rho \frac{d\boldsymbol{V}^*}{dt^*} = -\nabla p^* + \nabla . \boldsymbol{S}^* + \boldsymbol{J}^* \times \boldsymbol{B}^*, \tag{2}$$

In equation (2) uses the symbols are $\mathbf{V}^*$, ρ, p^* and d/dt^*, which stand for velocity, density, pressure, and significant derivative, respectively. Specifically, **B** is referred to as the total magnetic field and is defined as $\boldsymbol{B}^* = \boldsymbol{B}_0^* + b$, where *b* is the induced magnetic field and $\boldsymbol{B}_0^*$ is the applied magnetic field. $\boldsymbol{J}^*$ is referred to as the current density in this context. We disregard the induced magnetic field because we assume that the magnetic diffusivity is relatively great. As a result, the total magnetic field that is affecting the fluid is $\boldsymbol{B}_0^*$. We also presume in the current investigation that no electric field is used.

In Eq. (2) $\boldsymbol{S}^*$ is the extra tensor of the Oldroyd 4-constant model which is defined as [31]

$$\mathbf{S}^* + \lambda_1^* \frac{D\mathbf{S}^*}{Dt^*} + \lambda_3^* tr\left(\mathbf{S}^*\right)\mathbf{A}_1^* = \mu\left(1 + \lambda_2^* \frac{D}{Dt^*}\right)\mathbf{A}_1^*, \tag{3}$$

where $\mathbf{A}_1^*$, and DS^*/Dt^* are the first Rivilin-Ericksen tensor and upper convected derivative defined as

$$\mathbf{A}_1^* = \nabla\mathbf{V}^* + (\nabla\mathbf{V}^*)^{\mathbf{T}}, \tag{4}$$

$$\frac{D\mathbf{S}^*}{Dt^*} = \frac{d\mathbf{S}^*}{dt^*} - (\nabla\mathbf{V}^*)\mathbf{S}^* - \mathbf{S}^*(\nabla\mathbf{V}^*)^{\mathbf{T}}. \tag{5}$$

Figure 1 demonstrates the flow geometry of the calendering process. We take the viscoelastic incompressible fluid flow with the presence of the MHD among two identical rolls having the same radii *R is* considered. Identical rolls rotate in the anticlockwise direction by means of

rotation having speed *N*, with a uniform velocity of every roll that is $U^* = RN$. Let $2H_0$ denote the smallest gap between the rolls. At point $x^* = -x_f^*$, the molten polymer's initial width of $2H_f$ makes its first contact with the rolls. At point $x = x_0^*$, the final sheet separates from the rolls. As shown in Fig. 1, let u^* and v^* represent the in x^* and y^* directions components of velocity, respectively. where the magnetic field is applied along y^**-axis*. In the analysis of calendering the space between two rolls is very small as compared to the diameter of the rolls i.e. $H_0/R << 1$. Therefore the lubrication approximation may be used in the current analysis i.e. $v^* << u^*$ and $\frac{\partial}{\partial x^*} << \frac{\partial}{\partial y^*}$.

The velocity field for two-dimensional flow is provided as

$$\mathbf{V}^* = \left[u^*\left(x^*, y^*\right), v^*\left(x^*, y^*\right)\right]. \tag{6}$$

The molten polymer is experiences a uniform magnetic field applied in the longitudinal direction. Given the very small values of the magnetic so that the induced magnetic field is ignored. The magnetohydrodynamics(MHD) Lorentz force caused by the exerted magnetic field takes the form [40-43]

$$\boldsymbol{J}^* \times \boldsymbol{B}^* = \left[-\sigma B_0^2 u^*, 0, 0\right]. \tag{7}$$

In the above relation B_0^* is the magnetic field and σ is said to be the electric conductivity of the fluid.

By using the velocity field and Eq. (7) in the equations (1-3), one can get

$$\frac{\partial u^*}{\partial x^*} + \frac{\partial v^*}{\partial y^*} = 0, \tag{8}$$

$$\rho\left(u^* \frac{\partial u^*}{\partial x^*} + v^* \frac{\partial u^*}{\partial y^*}\right) = -\frac{\partial p^*}{\partial x^*} + \frac{\partial S^*_{x^*x^*}}{\partial x^*} + \frac{\partial S^*_{x^*y^*}}{\partial y^*} - \sigma B_0^2 u^*, \tag{9}$$

$$\rho\left(u^* \frac{\partial v^*}{\partial x^*} + v^* \frac{\partial v^*}{\partial y^*}\right) = -\frac{\partial p^*}{\partial y^*} + \frac{\partial S^*_{x^*y^*}}{\partial x^*} + \frac{\partial S^*_{y^*y^*}}{\partial y^*}, \ , \tag{10}$$

$$S^*_{x^*x^*}+\lambda_1^*\left[\left(u^*\frac{\partial}{\partial x^*}+v^*\frac{\partial}{\partial y^*}\right)S^*_{x^*x^*}-2\frac{\partial u^*}{\partial x^*}S^*_{x^*x^*}-2\frac{\partial u^*}{\partial y^*}S^*_{x^*y^*}\right]+2\lambda_3^*\left(S^*_{x^*x^*}+S^*_{y^*y^*}\right)\frac{\partial u^*}{\partial x^*}=2\mu\frac{\partial u^*}{\partial x^*}$$
$$+2\mu\lambda_2^*\left[\left(u^*\frac{\partial}{\partial x^*}+v^*\frac{\partial}{\partial y^*}\right)\frac{\partial u^*}{\partial x^*}-2\left(\frac{\partial u^*}{\partial x^*}\right)^2-\frac{\partial u^*}{\partial y^*}\left(\frac{\partial u^*}{\partial y^*}+\frac{\partial v^*}{\partial x^*}\right)\right],\tag{11}$$

$$S^*_{x^*y^*}+\lambda_1^*\left[\left(u^*\frac{\partial}{\partial x^*}+v^*\frac{\partial}{\partial y^*}\right)S^*_{x^*y^*}-\frac{\partial v^*}{\partial x^*}S^*_{x^*x^*}-\frac{\partial u^*}{\partial y^*}S^*_{y^*y^*}\right]+\lambda_3^*\left(S^*_{x^*x^*}+S^*_{y^*y^*}\right)\left(\frac{\partial u^*}{\partial y^*}+\frac{\partial v^*}{\partial x^*}\right)=$$
$$\mu\left(\frac{\partial u^*}{\partial y^*}+\frac{\partial v^*}{\partial x^*}\right)+\mu\lambda_2^*\left[\left(u^*\frac{\partial}{\partial x^*}+v^*\frac{\partial}{\partial y^*}\right)\left(\frac{\partial u^*}{\partial y^*}+\frac{\partial v^*}{\partial x^*}\right)-2\left(\frac{\partial u^*}{\partial x^*}\frac{\partial v^*}{\partial x^*}+\frac{\partial u^*}{\partial y^*}\frac{\partial v^*}{\partial y^*}\right)\right],\tag{12}$$

$$S^*_{y^*y^*}+\lambda_1^*\left[\left(u^*\frac{\partial}{\partial x^*}+v^*\frac{\partial}{\partial y^*}\right)S^*_{y^*y^*}-2\frac{\partial v^*}{\partial x^*}S^*_{x^*y^*}-2\frac{\partial v^*}{\partial y^*}S^*_{y^*y^*}\right]+2\lambda_3^*\left(S^*_{x^*x^*}+S^*_{y^*y^*}\right)\frac{\partial v^*}{\partial y^*}=2\mu\frac{\partial v^*}{\partial y^*}$$
$$+2\mu\lambda_2^*\left[\left(u^*\frac{\partial}{\partial x^*}+v^*\frac{\partial}{\partial y^*}\right)\frac{\partial v^*}{\partial x^*}-2\left(\frac{\partial v^*}{\partial y^*}\right)^2-\frac{\partial v^*}{\partial x^*}\left(\frac{\partial v^*}{\partial x^*}+\frac{\partial u^*}{\partial y^*}\right)\right].\tag{13}$$

The flow is symmetric about the central line so, the mathematical expression of this boundary condition is follow as

$$\frac{\partial u^*}{\partial y^*}=0,\quad \text{at } y^*=0,\tag{14}$$

On the upper wall of the roll surface, we introduced the slip condition, which is defined in mathematical form as [16, 29],

$$u^*=U^*-\gamma^*S^*_{x^*y^*},\quad \text{at } y^*=h,\tag{15}$$

To made flow equations and boundary conditions in dimensionless form, introducing the normalized variables and parameters as.

$$y=\frac{y^*}{H_0},\ \frac{h\left(x^*\right)}{H_0}=1+x^2,\ p=\sqrt{\frac{H_0}{2R}}\frac{H_0 p_c^*}{\left(\mu+\eta\right)U^*},\ x=\frac{x^*}{\sqrt{2RH_0}},\ u\left(x,y\right)=\frac{u^*\left(x^*,y^*\right)}{U^*},$$
$$\lambda=\frac{x_0^*}{\sqrt{2RH_0}},\ Re=\rho U^* H_0/\mu,\ \beta=\sqrt{\frac{H_0}{2R}},\ \ v\left(x,y\right)=\sqrt{\frac{2R}{H_0}}\frac{v^*\left(x^*,y^*\right)}{U^*},$$
$$\mathbf{S}=\mathbf{S}^*\frac{H_0}{\mu U^*},\ \lambda_1=\frac{\lambda_1^* U^*}{H_0},\ \lambda_2=\frac{\lambda_2^* U^*}{H_0},\ \lambda_3=\frac{\lambda_3^* U^*}{H_0}. \tag{16}$$

Using Eq. (16) into Eqs. (8-15), we arrived the following equations.

$$\frac{\partial u}{\partial x}+\frac{\partial v}{\partial y}=0, \tag{17}$$

$$\mathrm{Re}\,\beta\left(u\frac{\partial u}{\partial x}+v\frac{\partial u}{\partial y}\right)=-\frac{\partial p}{\partial x}+\beta\frac{\partial S_{xx}}{\partial x}+\frac{\partial S_{xy}}{\partial y}-Ha^2 u, \tag{18}$$

$$\mathrm{Re}\,\beta^3\left(u\frac{\partial v}{\partial x}+v\frac{\partial v}{\partial y}\right)=-\frac{\partial p}{\partial y}+\beta^2\frac{\partial S_{xy}}{\partial x}+\beta\frac{\partial S_{yy}}{\partial y}, \tag{19}$$

$$S_{xx}+\lambda_1\left[\beta\left(u\frac{\partial}{\partial x}+v\frac{\partial}{\partial y}\right)S_{xx}-2\beta\frac{\partial u}{\partial x}S_{xx}-2\frac{\partial u}{\partial y}S_{xy}\right]+2\beta\lambda_3\left(S_{xx}+S_{yy}\right)\frac{\partial u}{\partial x}=2\beta\frac{\partial u}{\partial x}$$
$$+2\lambda_2\left[\beta^2\left(u\frac{\partial}{\partial x}+v\frac{\partial}{\partial y}\right)\frac{\partial u}{\partial x}-2\beta^2\left(\frac{\partial u}{\partial x}\right)^2-\frac{\partial u}{\partial y}\left(\frac{\partial u}{\partial y}+\beta^2\frac{\partial v}{\partial x}\right)\right], \tag{20}$$

$$S_{xy}+\lambda_1\left[\beta\left(u\frac{\partial}{\partial x}+v\frac{\partial}{\partial y}\right)S_{xy}-\beta^2\frac{\partial v}{\partial x}S_{xx}-\frac{\partial u}{\partial y}S_{yy}\right]+\lambda_3\left(S_{xx}+S_{yy}\right)\left(\frac{\partial u}{\partial y}+\beta^2\frac{\partial v}{\partial x}\right)=$$
$$\left(\frac{\partial u}{\partial y}+\beta^2\frac{\partial v}{\partial x}\right)+\lambda_2\left[\beta\left(u\frac{\partial}{\partial x}+v\frac{\partial}{\partial y}\right)\left(\frac{\partial u}{\partial y}+\beta^2\frac{\partial v}{\partial x}\right)-2\beta^2\left(\beta\frac{\partial u}{\partial x}\frac{\partial v}{\partial x}+\frac{\partial u}{\partial y}\frac{\partial v}{\partial y}\right)\right], \tag{21}$$

$$S_{yy}+\lambda_1\left[\beta\left(u\frac{\partial}{\partial x}+v\frac{\partial}{\partial y}\right)S_{yy}-2\beta^2\frac{\partial v}{\partial x}S_{xy}-2\beta\frac{\partial v}{\partial y}S_{yy}\right]+2\beta\lambda_3\left(S_{xx}+S_{yy}\right)\frac{\partial v}{\partial y}=2\beta\frac{\partial v}{\partial y}$$
$$+2\lambda_2\left[\beta^2\left(u\frac{\partial}{\partial x}+v\frac{\partial}{\partial y}\right)\frac{\partial v}{\partial y}-2\beta^2\left(\frac{\partial v}{\partial y}\right)^2-\beta^2\frac{\partial v}{\partial x}\left(\beta^2\frac{\partial v}{\partial x}+\frac{\partial u}{\partial y}\right)\right]. \tag{22}$$

$$\frac{\partial u}{\partial y}=0,\quad \text{at } y=0, \tag{23}$$

$$u = 1 - KnS_{xy}, \text{ at } y = 1 + x^2, \tag{24}$$

where $Kn = \gamma^* / H_0$ is known as the slip coefficient and $Ha = \sqrt{\sigma/\mu} B_0 H_0$ denote the Hartmann number

3. Resolution Method

Figure 2 shows the dimensionless physical parameter. Most physical changes in the calendering process occur in the narrow gap between the two rolls. In the current study, our primary attention is to study the influence of the involved parameters in the nip region. As Reynolds number is very small in the minimal region because in this region the distance between the two rolls is very minor as associated with the radius of the rolls. Furthermore, in the calendering procedure, the Reynolds is considered to be small (i.e., less than the unity) and β is the ratio of the nip gap and radius of the cylinders (which is also less than unity). These suppositions permit us to drop the expressions, which includes of β and *Re* so the above equations can be written as;

$$-\frac{\partial p}{\partial x} + \frac{\partial S_{xy}}{\partial y} - Ha^2 u = 0, \tag{25}$$

$$\frac{\partial p}{\partial y} = 0, \tag{26}$$

$$S_{xx} - 2\lambda_1 \frac{\partial u}{\partial y} S_{xy} = 2\lambda_2 \left(\frac{\partial u}{\partial y} \right)^2, \tag{27}$$

$$S_{xy} + \lambda_3 S_{xx} \frac{\partial u}{\partial y} = \frac{\partial u}{\partial y}, \tag{28}$$

$$S_{yy} = 0, \tag{29}$$

$$S_{xy} = \left\{ \frac{1 + 2\alpha_1 \left(\partial u / \partial y \right)^2}{1 + 2\alpha_2 \left(\partial u / \partial y \right)^2} \right\} \frac{\partial u}{\partial y}. \tag{30}$$

where $\alpha_1 = \lambda_2 \lambda_3$ and $\alpha_2 = \lambda_1 \lambda_3$. Equation (26) demonstrates that pressure is a variables of *x*, to get rid from pressure in Equation (25), differentiating Equation (25) with respect to *y*.

$$\frac{\partial^2 S_{xy}}{\partial y^2} - Ha^2 \frac{\partial u}{\partial y} = 0, \tag{31}$$

By using the value of S_{xy} into equation (31), we get

$$\frac{\partial^2}{\partial y^2}\left[\left\{\frac{1+2\alpha_1\left(\partial u/\partial y\right)^2}{1+2\alpha_2\left(\partial u/\partial y\right)^2}\right\}\frac{\partial u}{\partial y}\right]-Ha^2\frac{\partial u}{\partial y}=0. \tag{32}$$

We offer the stream function as [30-31] to address the issue quantitatively.

$$u=\frac{\partial \psi}{\partial y},\ v=-\frac{\partial \psi}{\partial x}. \tag{33}$$

Using Eq. (33) into Eqs. (25) and (32), we get

$$\frac{dp}{dx}=\frac{\partial}{\partial y}\left[\left\{\frac{1+2\alpha_1\left(\partial^2\psi/\partial y^2\right)^2}{1+2\alpha_2\left(\partial^2\psi/\partial y^2\right)^2}\right\}\frac{\partial^2\psi}{\partial y^2}\right]-Ha^2\frac{\partial \psi}{\partial y}. \tag{34}$$

$$\frac{\partial^2}{\partial y^2}\left[\left\{\frac{1+2\alpha_1\left(\partial^2\psi/\partial y^2\right)^2}{1+2\alpha_2\left(\partial^2\psi/\partial y^2\right)^2}\right\}\frac{\partial^2\psi}{\partial y^2}\right]-Ha^2\frac{\partial^2\psi}{\partial y^2}=0. \tag{35}$$

The relevant condition in term of stream function is defined as

$$\frac{\partial^2\psi}{\partial y^2}=0,\quad \text{at } y=0, \tag{36}$$

$$\frac{\partial \psi}{\partial y}=1-KnS_{xy},\ \text{at } y=1+x^2, \tag{37}$$

We need two extra boundary conditions to solve Eq. (35) together with (36) and (37). For this, we used the dimensionless form of the volume metric flow equation to find these additional conditions.

$$1+\lambda^2=\int_0^h u dy, \tag{38}$$

where $1+\lambda^2=Q/\left(2UH_0\right)$ dimensionless flow rate[11, 20-23].

Eq. (38) in terms of stream function

$$1+\lambda^2=\int_0^h \frac{\partial \psi}{\partial y}dy,$$

$$1+\lambda^2=\psi(h)-\psi(0). \tag{39}$$

Equation (39) implies

$$\left.\begin{aligned}\psi(0)&=0, \text{ at } y=0\\ \psi(h)&=1+\lambda^2 \text{ at } y=1+x^2\end{aligned}\right\}. \tag{40}$$

Middleman [32] defined constraint on pressure gradient and pressure as follows.

$$\frac{dp}{dx}=p=0 \text{ at } x=x_0, \tag{41}$$

$$p=0 \text{ at } x=-x_f. \tag{42}$$

In the current scenario equation (35) is non-linear fourth order differential equation. Therefore analytical solution of equation (35) into possible, we solved this problem by applying Matlab's built-in "bvp4c" method [30, 31]. After calculated the stream function values numerically we use these values in equation (34) to find out the pressure gradient.
In order to get pressure, one can integrate pressure gradient using the Runge-Kutta fourth-order technique as use many researcher in their research [16, 17, 20-23]

$$p=\int_{\lambda}^{x}\frac{dp}{dx}dx. \tag{43}$$

Utilizing the formula $x_f=\left(H_f/H_0-1\right)^{1/2}$ as specified by Middleman [11, 12], the entering sheet thickness $\left(H_f/H_0\right)$ can be calculated.

The most prominent mechanical quantities use in the calendering process are defined as

Roll-separating force and power transferred to the fluid are expressed as [11,20]

$$\frac{F}{W}(\alpha_2)=\frac{\mu UR}{H_0}\Pi(\alpha_2), \tag{44}$$

$$\dot{W}(\alpha_2)=WU^2\mu\sqrt{\frac{R}{H_0}}\Gamma(\alpha_2), \tag{45}$$

where

$$\Pi(\alpha_2)=\int_{-x_f}^{\lambda}\left[\int_{x}^{\lambda}\Im(\alpha_2)dx\right]dx, \tag{45}$$

$$\Gamma(\alpha_2) = 2\sqrt{2}\int_{-x_f}^{\lambda} \Im(\alpha_2)(1+x^2)dx, \tag{47}$$

$$\Im(\alpha_2) = \frac{\partial}{\partial y}\left[\left\{ \frac{1+2\alpha_1(\partial u/\partial y)^2}{1+2\alpha_2(\partial u/\partial y)^2} \right\} \frac{\partial u}{\partial y} \right]. \tag{48}$$

We validated our numerical results with the Middleman [11] for Newtonian fluid and Ali et al [31] paper as presented in figure 3(a, b) for pressure curves. Our numerical results consistent Newtonian scenario [11] for, $\alpha_1 \to \alpha_2$ *and* $Ha = kn = 0,$ as well as Atif et al. [31], where $\alpha_1 = 3, \alpha_2 = 2$ *and* $Ha = kn = 0$.

4. Graphical results and their explanations

In this section we demonstrated numerical results through graphs how polymer sheet velocity, pressure gradient pressure and mechanical variables of calendering process are affected with involved parameters such as slip coefficient (*Kn*), Hartman number (*Ha*) and non-Newtonian fluid parameters.

The influence of the Hartmann number on the polymer sheet velocity is presented in Figure 4(a, b) at two different cross section i.e. *x=-0.6 and x=0.1* within the intervals $[-x_f, -\lambda]$ (upstream region) and $[-\lambda, \lambda]$ (downstream region) for fixed values of *Kn = 0.2*. Figure 4a depicts that the velocity of the molten sheet at position x = -0.6(where *dp*/*dx*>0) in upstream region is an increases in the central area of the rolls, while its decreases near the rolls surface, as the values of the Hartmann number increases from 0 to 5. Figure 4b depicts that the velocity of molten sheet at position *x = 0.1*(where *dp/dx*<0) in downstream region show decreases trend in nip region while it increases near the rolls surface.

How the slip parameter (*Kn*) impacts the velocity profile at *x=-0*.6 in the interval $[-x_f, -\lambda]$, where $dp/dx > 0$ for fixed values of $\lambda = 0.440$, $\alpha_1 = 0.5, \alpha_2 = 2$ *and* $Ha = 2$ is depicted in figure 5a. On rising slip parameter (*Kn*), the velocity distribution in this figure demonstrates an increase trend in the middle plane. The velocity of the molten sheet is opposite when it is close to the roll surface (decreases). Moreover, Figure 5b demonstrates that, for increasing slip parameter (*Kn*), velocity decreases towards the roll surface. As the slip parameter (*Kn*) is increased, figure 5b demonstrates that the velocity distribution grows in the center of the plane, while decreasing at the roll surface at the position $x = 0.1$ in downstream region $[-\lambda, \lambda]$ (where *dp/dx<0*).

The pressure curves against x for the different values of the Hartmann number (*Ha*), slip parameter (*Kn*), α_1 and α_2 are plotted in figures 6-8 with exiting points $\lambda = 0.2923$ and $\lambda = 0.440$ respectively. Figures 6(a, b) demonstrate the influence of the Hartmann number (*Ha*) on pressure, while Figures 7(a, b) demonstrate the influence of the slip parameter (*Kn*) on pressure. According to the boundary condition (41), all figures demonstrate that the pressure begins at zero at $x = \lambda$ and continuously enhancing and gain its maximum values at $x = -\lambda$ and then continuously decreasing until it goes to zero at $x = -x_f$ (the point where sheet contact the roll first time), when we move from right to left on *x*-axis. Both figure 6(a, b) reveals that the magnitude of pressure is grater for flow rate value ($\lambda = 0.440$) as compared to flow rate value ($\lambda = 0.2923$). One can see that the length of contact of molten sheet with roll extended with enhancing Hartmann number *(Ha).*

The pressure with *Ha = 0.2* and for two different flow $\lambda = 0.2923$ and 0.440 are affected by the slip parameter (*Kn*) varying from 0 to 0.4, as shown in figures 7(a, b). The influence of the slip parameter is opposite to the Hartmann number (*Ha*). Due to the boundary condition established (in Equation (41)), both figures show that all curves start at zero. Moving left from this point on the *axis*, the pressure grows and attains its maximum value at $x = -\lambda$, after this point the pressure shows decline trend and becomes zero at $x = -x_f$. (where the sheet contact the roll initially). It is obviously from figure 7(a, b), as the slip parameter (*Kn*) enhancing for 0 to 0.4, the pressure curves decreases and the pressure domain, or the area where the fluid touches the rolls, becomes smaller. Figure 7(a, b) exhibits that the maximum pressure decreases by 48% and 39%, when slip parameter value (*Kn = 0.4*) applied, compared to the no-slip condition (*Kn = 0*) for two different exit points $\lambda = 0.2923$ and $\lambda = 0.440$, while keeping other parameters fixed values $\alpha_1 = 0.5, \alpha_2 = 2$ *and* $Ha = 0.1$.

To illustrate how the pressure is affected by the $\alpha_1 and\ \alpha_2$, figure 8(a, b) is plotted with exiting point $\lambda = 0.440$. Both parameter shows opposite effects on the pressure profiles. When the values of α_1 increases from 0.2 to 2.5 it is noted from figure 8a that the magnitude of the pressure increases and the length of domain decreases, while in figure 8b the opposite behavior is noted when the values of α_2 increases from 0.5 to 2.5.

In figures 9 and 10 pressure gradient is computed numerically to show how the Hartmann number (*Ha),* slip parameter (*Kn*), $\alpha_1 and\ \alpha_2$ influence the pressure gradient. and Figures 9–10 plot the computed pressure gradient *dp/dx* versus *x* to examine how the Hartmann

parameter (*Ha*) from 0 to 0.4 and slip parameter (*kn*) from 0 to 0.4 impact the pressure gradient. Due to the boundary condition defined in equation (41), all of the pressure gradient curves start from zero at $x=\lambda$. Moving left from this point on the *x*-axis, the pressure gradient continues to decrease until it reaches its minimum value at $x=0$. From there, the pressure gradient increases until it reaches zero at $x=-\lambda$. As it passes this point, it keeps going up until it reaches its highest levels just before the entry point. The magnitude of the pressure gradient as well as the contact length between the polymer sheet and the rolls are increases as the Hartmann number(*Ha*) rises shown in figure 9(a, b).

Similarly, pressure gradient is plotted against *x* to see the influence of slip parameter (*Kn*), α_1 and α_2 in figure 10 (a-d). Figures 10(a, b, d) show that magnitude of the pressure gradient decreases with increasing the values of the slip parameter(*Kn*) and α_2 while in figure 10c the magnitude of the pressure gradient reduces with enhancing the values of the α_1. The length of contact of the molten sheet with rolls in figure 10 (a, b, d) increases with increasing the values of the Hartmann number (*Ha*) and (α_2), while in figure 10c its decreases with increases the values of α_1.

The mechanical quantities such as power function, roll-separating force, and sheet thickness are presented in this paragraph. The roll separation force against α_2 is shown in Figure 11. This figure demonstrates how the separation force reduces as the α_2 raises. Moreover, when the leave-off distance rises, the roll separation force increases.

Figure 12 depicts power usage as a function of α_2, it is evident from this figure that power function decreases as the range of the material parameter α_2 increases. Moreover, power function values increases with increasing the values of λ.

In figure 13, we have plotted leave-off distance versus entering sheet thickness different values of slip parameter (*Kn*). One can see that leave-off distance decreases with increasing the values of the slip parameter (*Kn*) and entering sheet thickness.

4 Conclusions

The current study deals with the combined effects of Hartmann number and slip parameters using the Oldroyd 4-constant fluid model during calendering process. The numerical solution to the problem is obtained through the stream function. The graphical effects of the material parameters together with slip and MHD parameters are presented in various quantities.

The principal conclusions are:

- As the Hartmann number (*Ha*) is increased, the pressure profile inside the calender grows along with the domain's length.
- The maximum pressure decreases by 48% and 39% when slip parameter value (*Kn = 0.4*) applied, compared to the no-slip condition (*Kn = 0*).
- The power function and roll separating force enhancing with increasing the values of the leave off distance.
- Exiting Sheet thickness behave decreasing trend with increasing the slip parameter values.
- We aim for this numerical solution to serve as a robust benchmark for more complicated two-dimensional non-isothermal analysis of the calendering problems.
- Furthermore, the present analysis could help in establishing correlation between theoretical results and experimental observations in the rheological calendering process.

Nomenclature

$\boldsymbol{V}^*$	Velocity field *(m/sec)*
ρ	Density (kg/m^3)
$\boldsymbol{S}^*$	Cauchy stress tensor (N/m^2)
p	Pressure(N/m^2)
λ_1^*, λ_3^*	relaxation time(s)
λ_2^*	Retardation time(s)
$\boldsymbol{A_1^*}$	first Rivilin-Ericksen tensor(N/m^2)
x_0^*	detachment point of sheet(m)
x_f^*	entering point of sheet(m)
R	roll radius(m)
λ	final sheet thickness(m)
$\boldsymbol{J}^*$	current density
μ	Viscosity(N.s/m^2)
$\boldsymbol{B}^*$	the magnetic field
Dimensionless parameter	

Ha	Hartman number
β	Geometric parameter
Re	*Reynolds number*
Kn	Slip parameter
α_1	Dimensionless parameter
α_2	Dimensionless parameter

References

1. Ardichvili, G. "An attempt at a rational determination of theambering of calender rolls", *Kautschuk,* **14,** pp.23–25 (1938).
2. Gaskell, R. E. "The calendering of plastic materials", *J. Appl. Mech.*, **17,** pp. 334 - 336(1950). https://doi.org/10.1115/1.4010136.
3. Bergen, J. T., and Scott, G. W. "Pressure distribution in calendering of plastic materials", *J. Appl. Mech.*, **18** pp. 101-106(1951). https://doi.org/10.1115/1.4010227.
4. Alston, W. W., and Astill, K. N. "An analysis for the calendering of non-Newtonian fluids", *J. Appl. Polym. Sci.*, **17**, pp. 3157-3174 (1973). https://doi.org/10.1002/app.1973.070171018.
5. Brazinsky, I., Cosway H. F., Valle, C. F., Jr, et al. "A theoretical study of liquid-film spread heights in the calendering of Newtonian and power law fluids", *J. Appl. Polym. Sci.*, **14**, pp. 2771–2784(1970). https://doi.org/10.1002/app.1970.070141111.
6. Paslay, P. R. "Calendering of viscoelastic materials", *J. Appl. Mech.*, **24**, pp. 602-608(1957). https://doi.org/10.1115/1.4011607.
7. Ehrmann, G., Takserman-Krozer, R., and Schenk'el G. "Non-Newtonian fluid flow between rotating cylinders", *Rheol. Acta*; **16**: pp. 240-247(1977). https://doi.org/10.1007/BF01523734.
8. Kiparissides, C., and Vlachopoulos, J. "Finite element analysis of calendering", *Polym. Eng. Sci.*; 16, pp. 712-719 (1976). DOI: 10.1002/pen.760161010.
9. Chong, J. S. "Calendering thermoplastic materials", *J. Appl. Polym. Sci*., **12,** 191(1968). https://doi.org/10.1002/app.1968.070120118.
10. McKelvey, J. M. "Polymer processing", *John Wiley and Sons, New York*, (1962).

11. Middleman, S. "Fundamentals of polymer processing", *McGraw-Hill, New York*, (1977).

12. Tadmor, Z., and Gogos C. G. "Principles of polymer processing", *John Wiley Sons, Haifa, Israel*, (1979).

13. Dobbels, F., and Mewis, J. "Non-isothermal nip flows in calendering operations", *Aiche. J.*, **23** pp. 224 - 232(1977). https://doi.org/10.1002/aic.690230304.

14. Luther, S., and Mewes, D. "Three-dimensional polymer flow in the calender bank", *Polym. Eng. Sci.*, **44,** 1642–1647(2004). https://doi.org/10.1002/pen.20162.

15. Sofou S., and Mitsoulis, E. "Calendering of pseudoplastic and viscoplastic Sheets of finite thickness", *J. Plast. Film. Sheet.*, **20,** pp.185–222 (2004). https://doi.org/10.1177/8756087904047660.

16. Mitsoulis, E., and Sofou, S. "Calendering pseudoplastic and viscoplastic fluids with slip at the roll surface", *J. App. Mech.*; **73**: pp. 291–299(2006). https://doi.org/10.1115/1.2083847.

17. Hernandez, A., Arcos, J.C., and Méndez, F., at al. "Effect of pressure-dependent consistency index on the exiting sheet thickness in the calendering of Newtonian fluids", *Appl. Math. Model.*; 37, pp.6952–6963(2013). https://doi.org/10.1016/j.apm.2013.02.010.

18. Arcos, J. C., Méndez, F., and Bautista, O. "Effect of temperature-dependent consistency index on the exiting sheet thickness in the calendering of power-law fluids", *Int. J. Heat Mass Transfer.*, **54**, pp. 3979–3986(2011). https://doi.org/10.1016/j.ijheatmasstransfer.2011.04.027.

19. Levine, L. Corvalan, C. M., Campanella O. H., et al. "A model describing the two-dimensional calendering of finite width sheets", *Chem. Eng. Sci.;* **57**, pp. 643–650(2002). https://doi.org/10.1016/S0009-2509(01)00410-9.

20. Ali, N., Javed, M. A. and Sajid, M. "Theoretical analysis of the exiting thickness of sheets in the calendering of FENE-P fluid", *J. Non-Newtonian Fluid Mech.*, **225**, pp. 28-36 (2015). https://doi.org/10.1016/j.jnnfm.2015.09.005.

21. Ali, N., Javed, M. A., and Atif, H. M. "Non-isothermal analysis of calendering using couple stress fluid", *J. Plast. Film. Sheet.*, **34**, pp. 358-381(2017). https://doi.org/10.1177/8756087917746454.

22. Sajid, M., Ali, N. and Javed, M. A. "An exact solution for the calendering analysis of a third-order fluid", *J. Plast. Film. Sheet.*, **33**, pp. 124–141(2016). https://doi.org/10.1177/8756087916635855.

23. Sajid, M., Siddique, H., Ali N., et al. "Calendering of non-isothermal Rabinowitsch fluid", *J. Polym. Eng.*, **38**, pp. 83–92(2018). https://doi.org/10.1515/polyeng-2016-0294.

24. Javed, M. A. Ali N. and Sajid M. "A theoretical analysis of the calendering of Ellis fluid", *J. Plast. Film. Sheet.*, **33,** pp. 207 - 226(2017). https://doi.org/10.1177/8756087916647998.

25. Javed, M. A., Ali, N., and Arshad, S. "Numerical analysis of the calendering process by using Giesekus fluid model", *J. Plast. Film Sheet*., **36**, pp.167–190 (2020). https://doi.org/10.1177/8756087919887999.

26. Javed, M. A., Ali, N., Arshad, S., et al. "Numerical approach for the calendering process using Carreau-Yasuda fluid model", *J. Plast. Film Sheet.*, **37**, pp. 312–337 (2021). https://doi.org/10.1177/8756087920988748.

27. Javed, M. A., Nasir, S., Ali, N., et al. "Mathematical simulation of the calendering process for non-Newtonian polymers", *J. Plast. Film Sheet.*, **38(3)**, pp.369-395(2022). https://doi.org/10.1177/87560879211066900

28. Javed, M. A., Ali, N., Arshad, S., et al. "Theoretical investigation of a fluid model in calendering process involving slip at the upper roll surface*", Z Angew Math Mech.; **103***, pp. 1-14(2023). https://doi.org/10.1002/zamm.202100406.

29. Javed, M. A., Akram, R., Nazeer, M., et al. "Heat transfer analysis of the non-Newtonian polymer in the calendering process with slip effects", *Int. J. Modern Phy. B.* **38**, pp. 2450105 (2024). https://doi.org/10.1142/S0217979224501054.

30. Javed, M. A., Asghar, Z., Atif, H. M., et al. "A computational study of the calendering processes using Oldroyd 8-constant fluid with slip effects", *Polym. polym. Compos.*, **31**, pp.1-12(2023). https://doi.org/10.1177/09673911231202888.

31. Atif, H. M., Ali. N., Javed, M. A., et al. "A numerical analysis of calendering of Oldroyd 4-constant fluid", *J. Polym. Eng.*, **38**, pp. 1007-1016(2018). https://doi.org/10.1515/polyeng-2018-0083.

32. Abbas, Z., and Khaliq, S. "Calendering analysis of non-isothermal viscous nanofluid containing Cu-water nanoparticles using two counter-rotating rolls", *J. Plast. Film Sheet.*, **37**, pp.182–204(2021). https://doi.org/10.1177/8756087920951614.

33. Abbas, Z., Naeem, A., and Khaliq, S. "Variation in final sheet thickness in case of Sutterby fluid during the calendering process", *J. Polym. Eng.*; **42**, pp. 467–476(2022). https://doi.org/10.1515/polyeng-2021-0368.

34. Abbas Z., Khaliq S., Ihsan, S., et al. "Final sheet thickness variation during the non-isothermal calendering process of rheological Prandtl fluid polymer", *J. Plast. Film Sheet.*, **39(4)**, pp.399-426 (2023). https://doi.org/10.1177/87560879231186783.

35. Nazeer, M., Hussain, F., Türkyılmazoğlu, et al. "Towards an approximate solution of highly viscous electro-osmotic flows in inclined channel: Applications in petroleum and gas engineering", J. *Magn. Magn. Mater.*, 170793(2023). https://doi.org/10.1016/j.jmmm.2023.170793.

36. Nazeer, M., Hussain, F., Turkyilmazoglu, et al. "Development of highly viscous multiphase fluid flows: forwards an approximate Analysis", *J. Comput. Biophys. Chem.*, **22(3)**, pp.371-381(2023). https://doi.org/10.1142/S2737416523400112.

37. Nazeer, M., Ahamdi, A. A. A., Alzaed, et al. "Impact of slip boundary conditions, magnetic force, and porous medium on blood flow of Jeffrey fluid", *ZAMM-Zeitschrift für Angewandte Mathematik und Mechanik*, ***102*(10)**, e202100218 (2022). https://doi.org/10.1002/zamm.202100218.

38. Nazir, M. W., Javed, T., Ali, N., et al. "Theoretical investigation of thermal analysis in aluminum and titanium alloys filled in nanofluid through a square cavity having the uniform thermal condition", *Int. J. Mod. Phys. B.*, ***36*(22)**, pp. 2250140(2022). https://doi.org/10.1142/S0217979222501405.

39. Ali, N., Nazeer, M., & Javed, T. "Finite element simulations of free convection flow inside a porous inclined cavity filled with micropolar fluid", *J. Porous Media.*, ***24***(2), pp. 57-75(2021). DOI:10.1615/JPorMedia.2020024977.

40. Hsiao, Kai-Long, "To promote radiation electrical MHD activation energy thermal extrusion manufacturing system efficiency by using Carreau-Nanofluid with parameters control method", *Energy, Elsevier*, **130(C)**, pp. 486-499(2017). https://doi.org/10.1016/j.energy.2017.05.004.

41. Kai-Long Hsiao, "Micropolar nanofluid flow with MHD and viscous dissipation effects towards a stretching sheet with multimedia feature", *Int. J. Heat Mass Tran.*, **112**, pp.983–990(2017). https://doi.org/10.1016/j.ijheatmasstransfer.2017.05.042.

42. Kai-Long Hsiao, "Stagnation electrical MHD nanofluid mixed convection with slip boundary on a stretching sheet", *Appl. Therm. Eng.*, **98,** pp.850–861(2016) https://doi.org/10.1016/j.applthermaleng.2015.12.138

43. Kai-Long Hsiao, "Combined electrical MHD heat transfer thermal extrusion system using Maxwell fluid with radiative and viscous dissipation effects", *Appl. Therm. Eng.*, **112**, pp.1281-1288(2017). https://doi.org/10.1016/j.applthermaleng.2016.08.208

44. Ragueb, H., & Mansouri, K. "Exact solution of the Graetz–Brinkman problem extended to non-Newtonian nanofluids flow in elliptical microchannels", *J. Eng Math.*, **140**, 10 (2023). https://doi.org/10.1007/s10665-023-10267-6

45. Ragueb H., Tahiri A., Behnous D., et al., "Irreversibilities and heat transfer in magnetohydrodynamic microchannel flow under differential heating", *Int. Commun. Heat Mass Transf.*, **149**, 107155 (2023). https://doi.org/10.1016/j.icheatmasstransfer.2023.107155

46. Nazeer, M., Hussain, F., Hameed, M. K., et al. "Development of mathematical modeling of multi-phase flow of Casson rheological fluid: Theoretical approach", *Chaos, Soliton Fract*, **150**, pp. 111198(2021). https://doi.org/10.1016/j.chaos.2021.111198

47. Nazeer, M., Alqarni, M. Z., Hussain, F., et al. "Computational analysis of multiphase flow of non-Newtonian fluid through inclined channel: heat transfer analysis with perturbation method", *Comput Part Mech*, **10**, pp. 1371-1381(2023). https://doi.org/10.1007/s40571-023-00569-y

48. Nazeer, M., Al-Zubaidi, A., Hussain, F., et al. "Thermal transport of two-phase physiological flow of non-Newtonian fluid through an inclined channel with flexible walls", *Case Stud Therm Eng*, **35**, pp. 102146(2022). https://doi.org/10.1016/j.csite.2022.102146

49. Nazeer, M., Irfan, M., Hussain, F., et al. "Analytical study of heat transfer rate of peristaltic flow in asymmetric channel with laser and magnetic effects: Remedy for autoimmune disease", *Int J Mod Phys B*, **37**(3), pp. 2350025(2023). https://doi.org/10.1142/S021797922350025X

50. Nazeer, M., Hussain, F., Ahmad, F., et al. "Multi-phase flow of Jeffrey fluid bounded within magnetized horizontal surface" *Surf Interfaces*, **22**, pp. 100846(2021). https://doi.org/10.1016/j.surfin.2020.100846

Dr. Muhammad Asif Javed is an associate professor at the Department of Mathematics, the University of Lahore, Gujrat campus Pakistan. He is currently involved in teaching at the graduate/post-graduate level and research activities. His research interest is in fluid dynamics, flows in polymer processing. He has published more than about 30 research articles in different peer reviewed international journals.

Dr. Hafiz Muhammad Atif is an assistant Professor at University of Sialkot, Pakistan. He is currently involved in teaching at the graduate/post-graduate level and research activities. His research interests include studying the flows in processes such as blade coating, calendering, roll-over web coating, both analytically and numerically.

Ms. Uzma Shehzadi has completed her M. Phil in Mathematics under the supervision of Dr. Muhammad Asif Javed from the University of Lahore, Gujrat campus Pakistan. Her field of research is to investigate the problems in the polymer processing.

Dr. Ahmed S. Sowayan is Professor in the department of Mechanical Engineering, Al Imam Mohammad Ibn Saud Islamic University Riyadh, Saudi Arabia. Dr. Sowayan is working in thermal systems and published more than 30 research papers in different journals. His area of research is heat transfer, nanofluids, thermal engineering and computational fluid mechanics.

Dr. Mubbashar Nazeer He completed his doctorate from the Department of Mathematics and Statistics in Applied Mathematics (Fluid Mechanics) at the International Islamic University Islamabad in July 2018. He has served as an Assistant Professor in the Department of Mathematics, Riphah International University Faisalabad Campus near two years. Now, he is working as an Assistant Professor in the Department of Mathematics, Institute of Arts and Sciences, Government College University Faisalabad, Chiniot Campus. His area of research is Cavity flows, Newtonian and non-Newtonian fluids, analytical and numerical methods, Bio-fluid mechanics, porous medium, heat and mass transfer analyses, and Computational Fluid Dynamics. He also received two research awards from national institutions.

Dr. Sami Ullah Khan is Associate Professor in the Namal University Mianwali Pakistan. Dr. Khan has published 430 research papers with impact factor 1500 plus. He is reviewer of more

than 70 impact factor journal. Dr Khan is guest editor of 4 impact factor journals. Dr Khan has been awarded as distinguish researcher from university.

Figure captions

Fig. 1. Diagram of a calender and its variables.

Fig. 2. Calendering geometry in dimensionless variables.

Fig. 3(a, b). Comparison of current numerical results to published work.

Fig. 4(a, b). Hartman number (*Ha*) effects on the velocity curve at *x = -0.6* and *x = 0.1*.

Fig. 5(a, b). Slip parameter (*Kn*) effects on the velocity curve at *x = -0.6* and *x = 0.1*.

Fig. 6(a, b). Hartman number (*Ha*) effects on pressure at two different exiting points.

Fig. 7(a, b). Slip number (*Kn*) effects on pressure profile at two different exiting points.

Fig. 8(a, b). Impact of (α_1)and (α_2) on the pressure profile.

Fig. 9(a, b). Hartman number (*Ha*) effects on pressure gradient.

Fig. 10(a-d). Effects of slip parameter (*Kn*), α_1 and α_2 on pressure gradient.

Fig. 11. Force function versus α_2.

Fig. 12. Power function versus α_2.

Fig. 13. Relationship between λ and H_f/H_0.

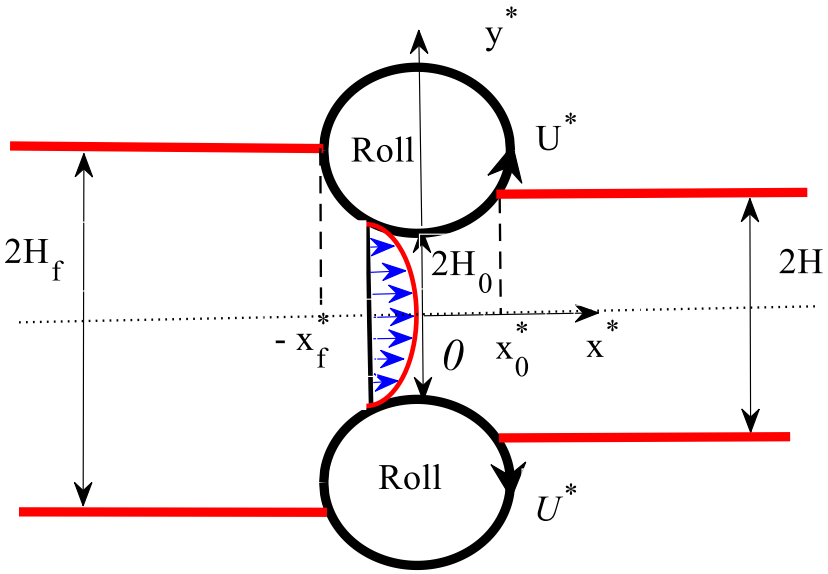

Fig. 1. Diagram of a calender and its variables.

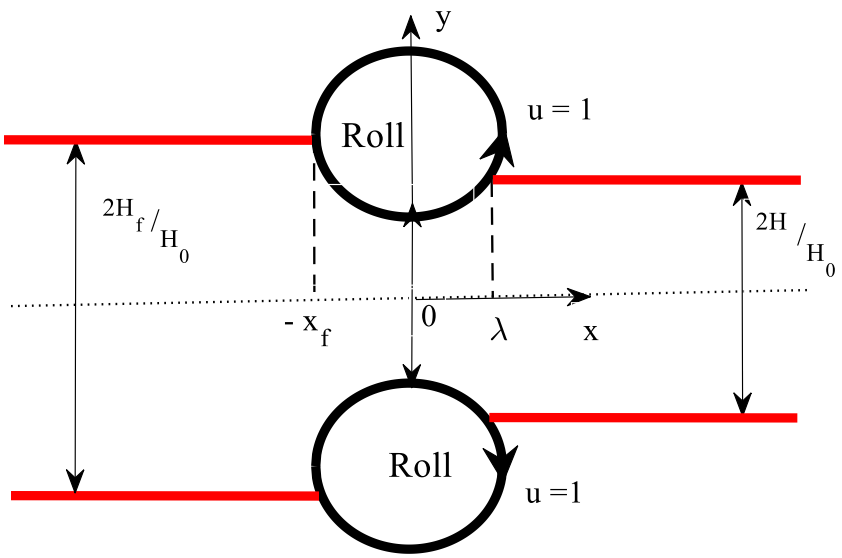

Fig. 2. Calendering geometry in dimensionless variables.

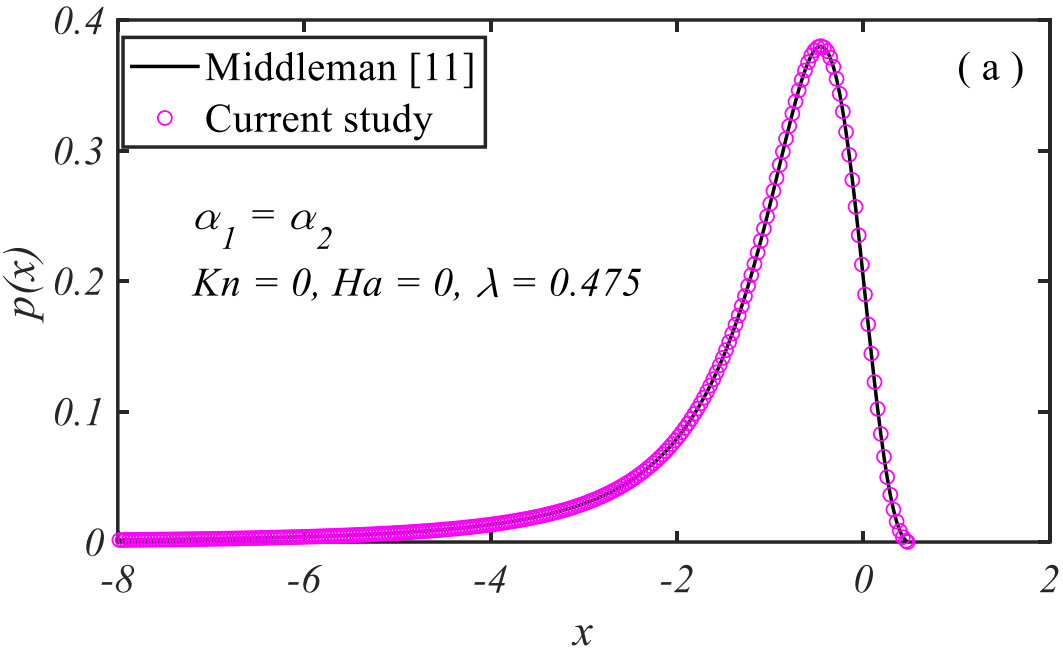

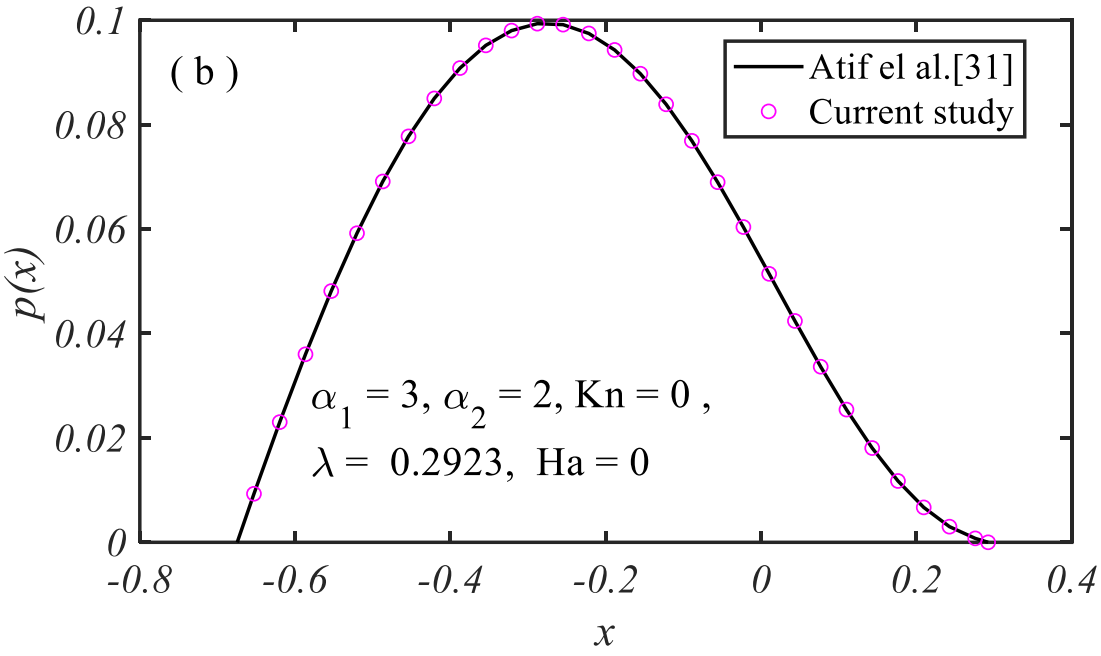

Fig. 3(a, b). Comparison of current numerical results to published work.

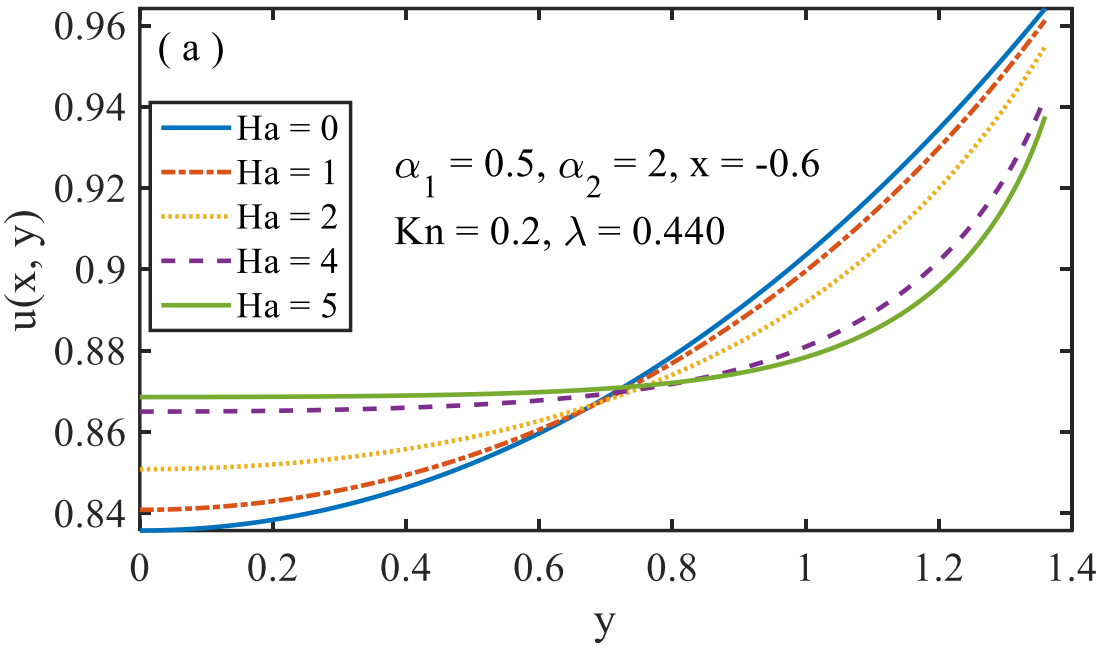

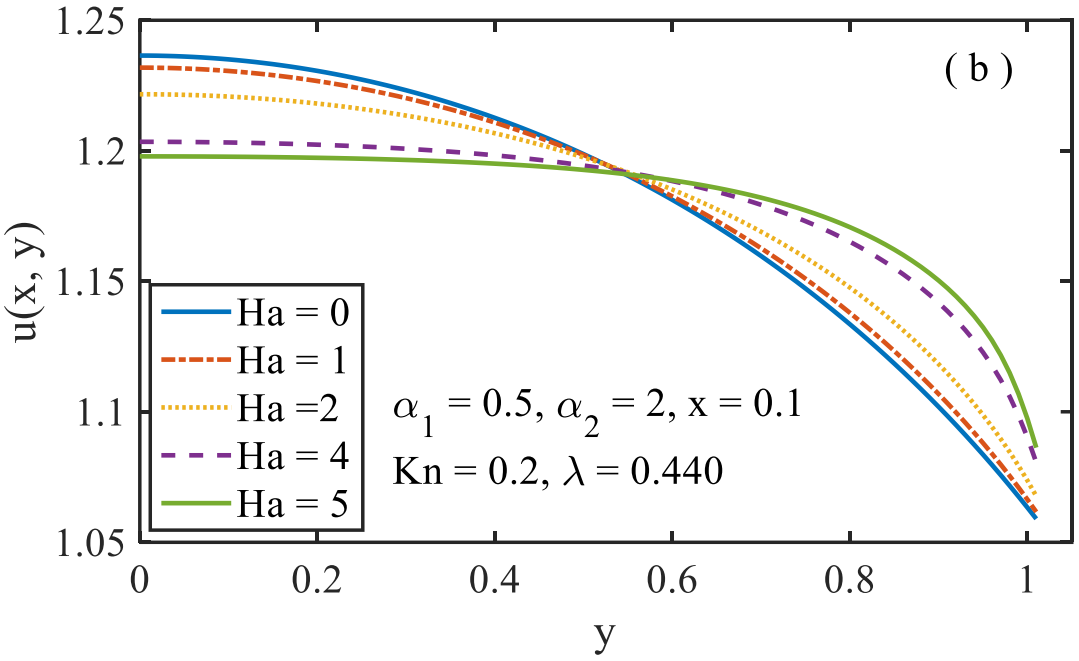

Fig. 4(a, b). Hartman number (*Ha*) effects on the velocity curve at *x = -0.6* and *x = 0.1*.

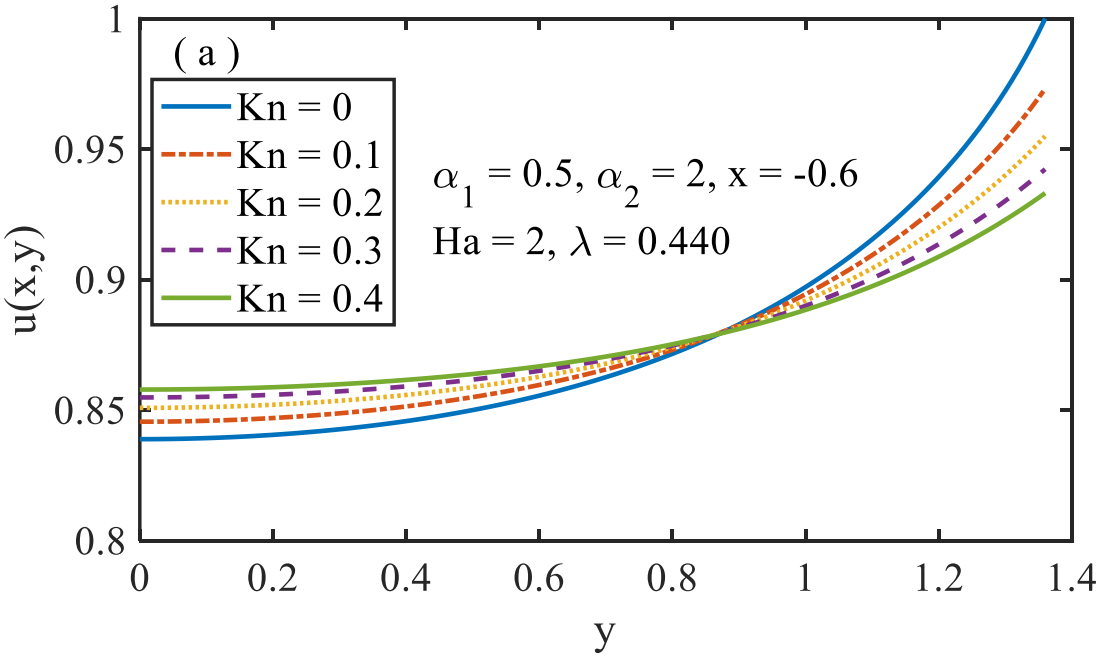

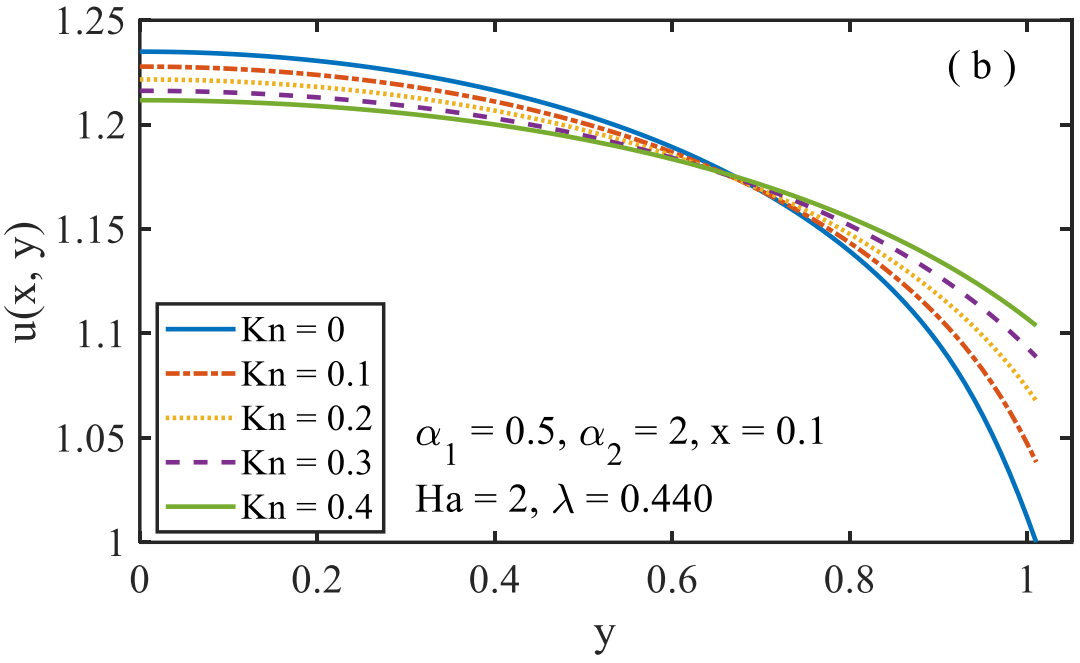

Fig. 5(a, b). Slip parameter (*Kn*) effects on the velocity curve at *x = -0.6* and *x = 0.1*.

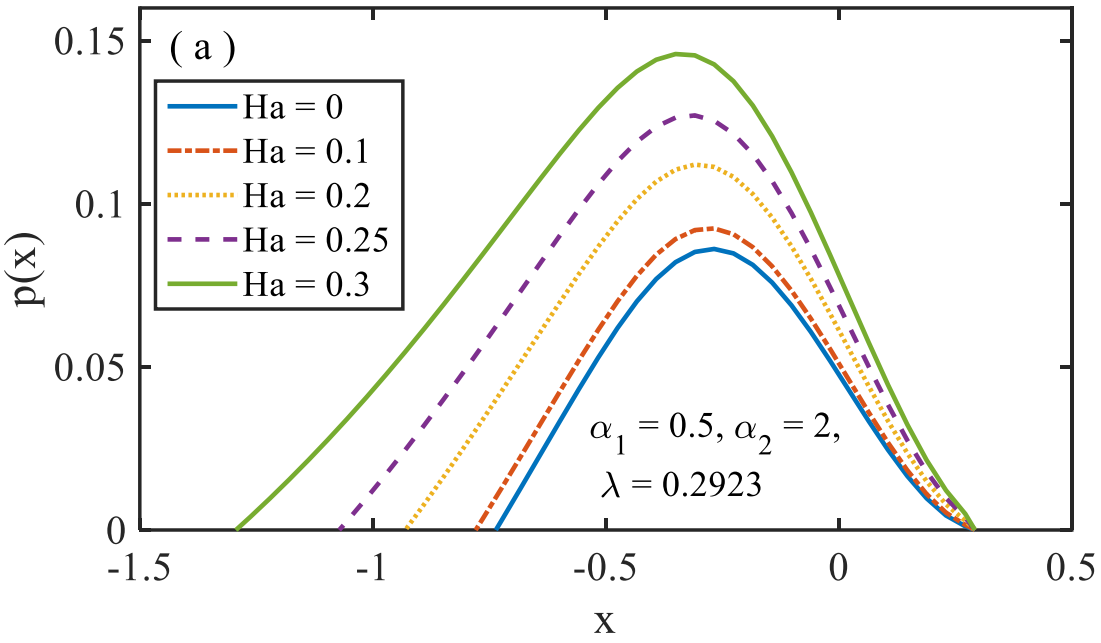

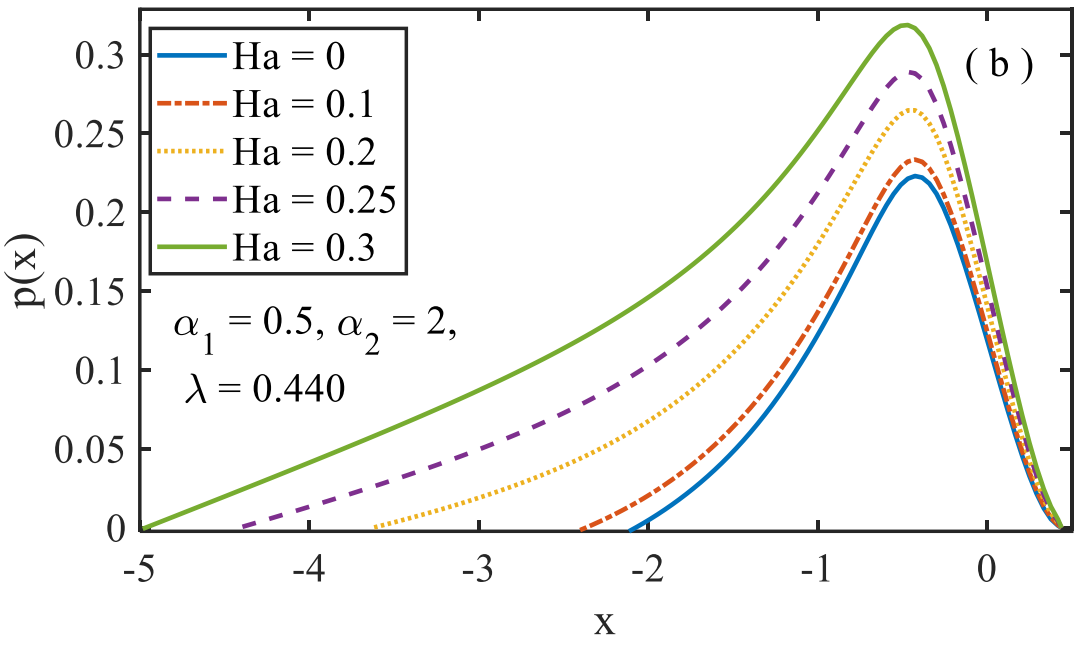

Fig. 6(a, b). Hartman number (*Ha*) effects on pressure at two different exiting points.

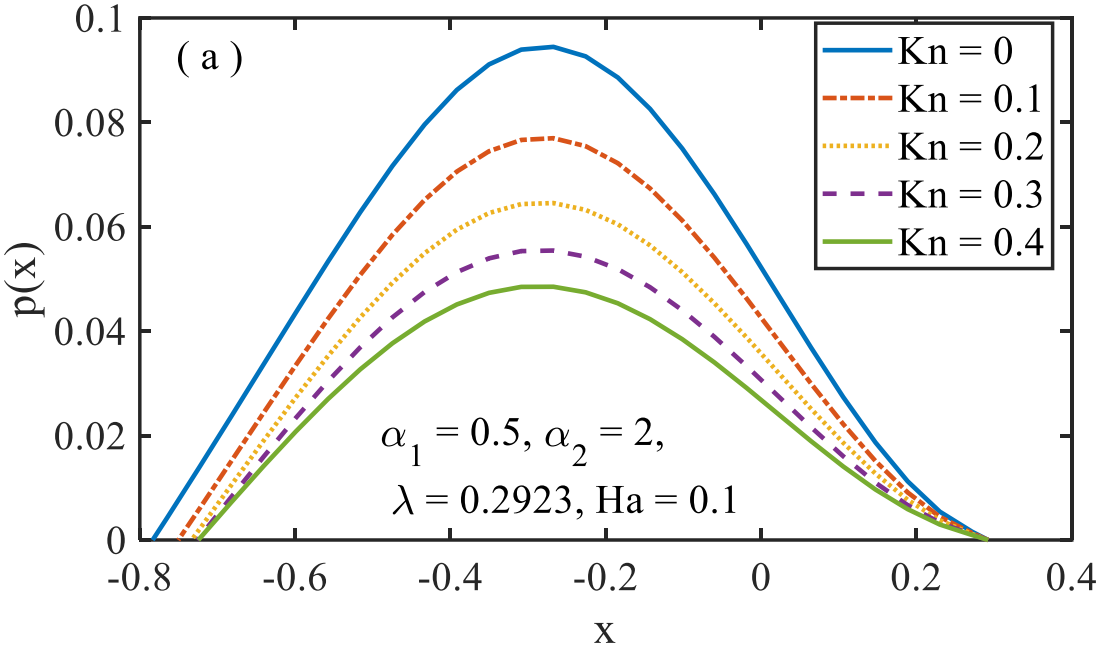

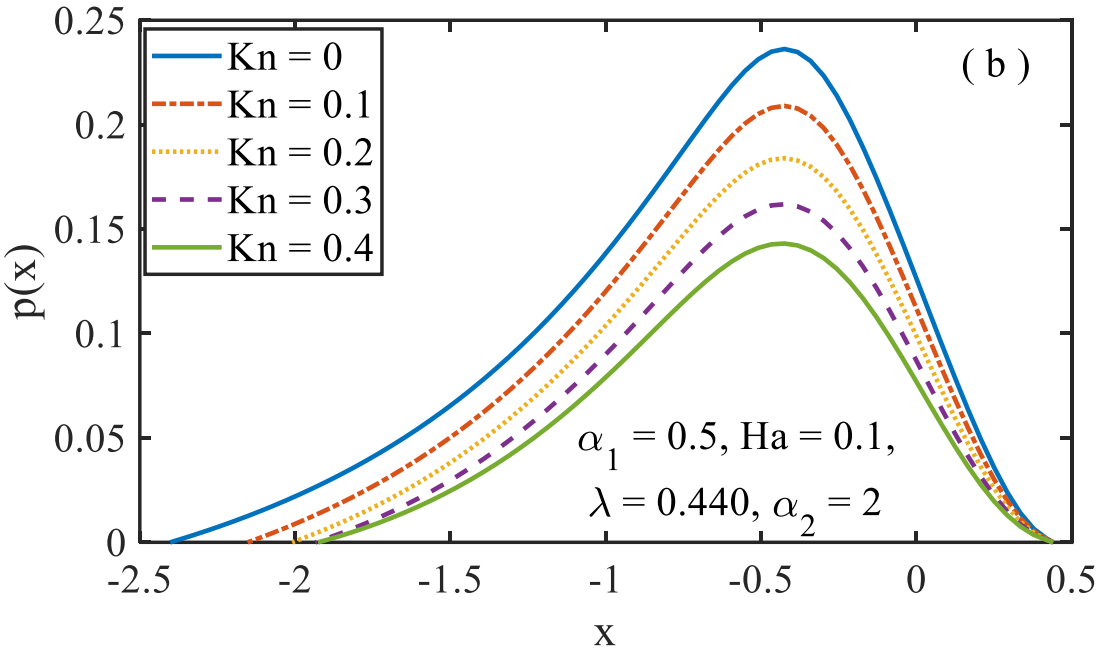

Fig. 7(a, b). Slip number (*Kn*) effects on pressure profile at two different exiting points

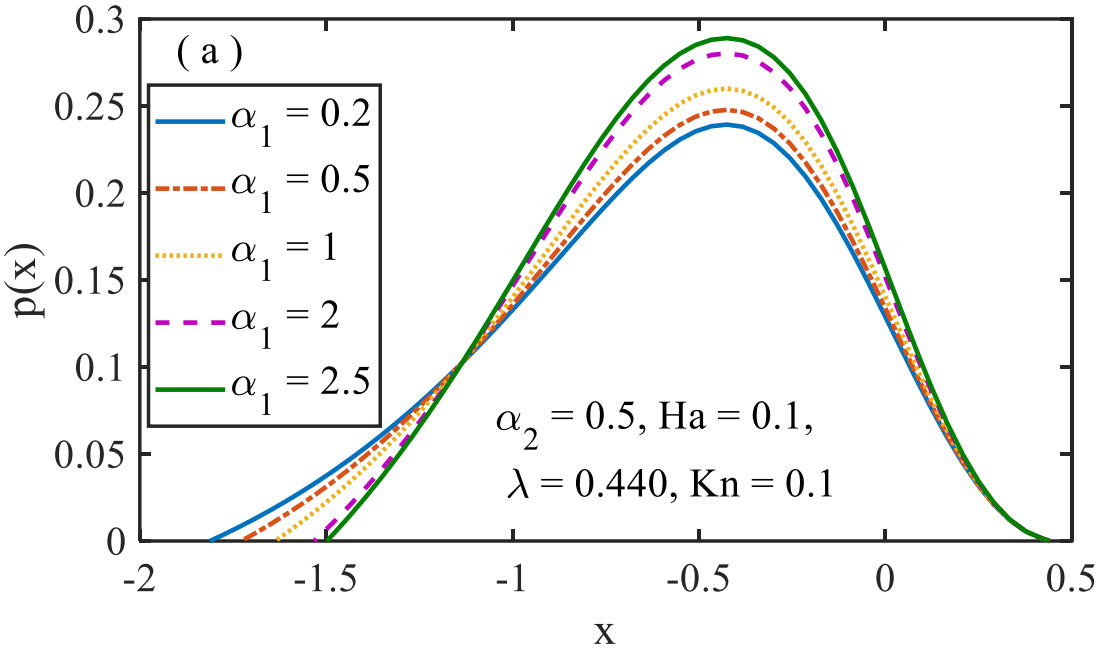

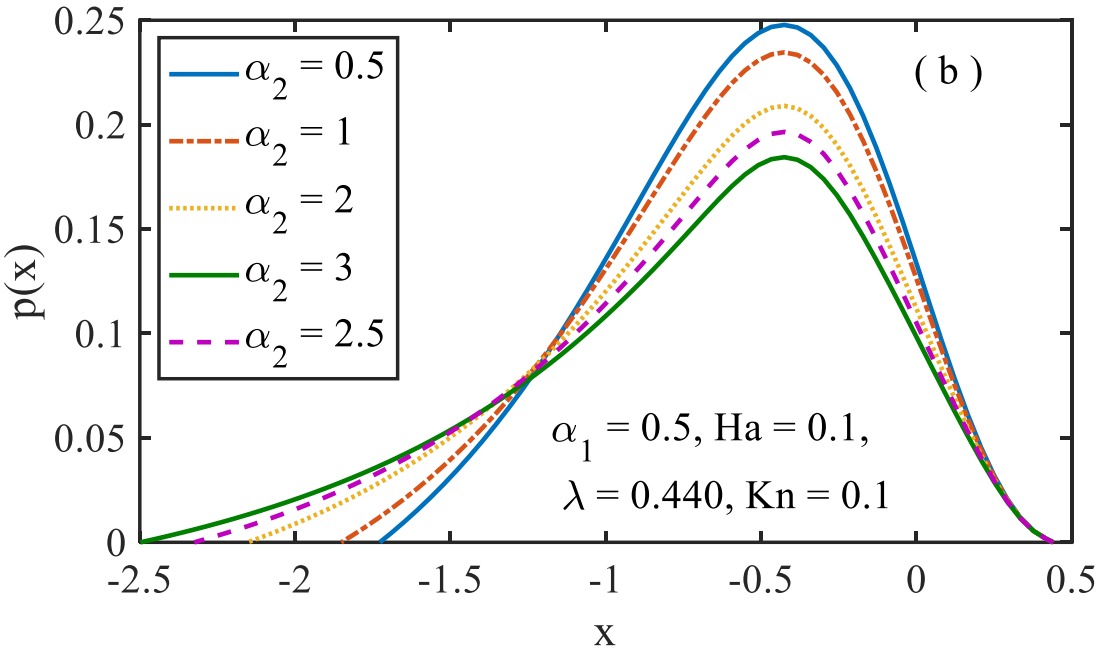

Fig. 8(a, b). Impact of (α_1) and (α_2) on the pressure profile.

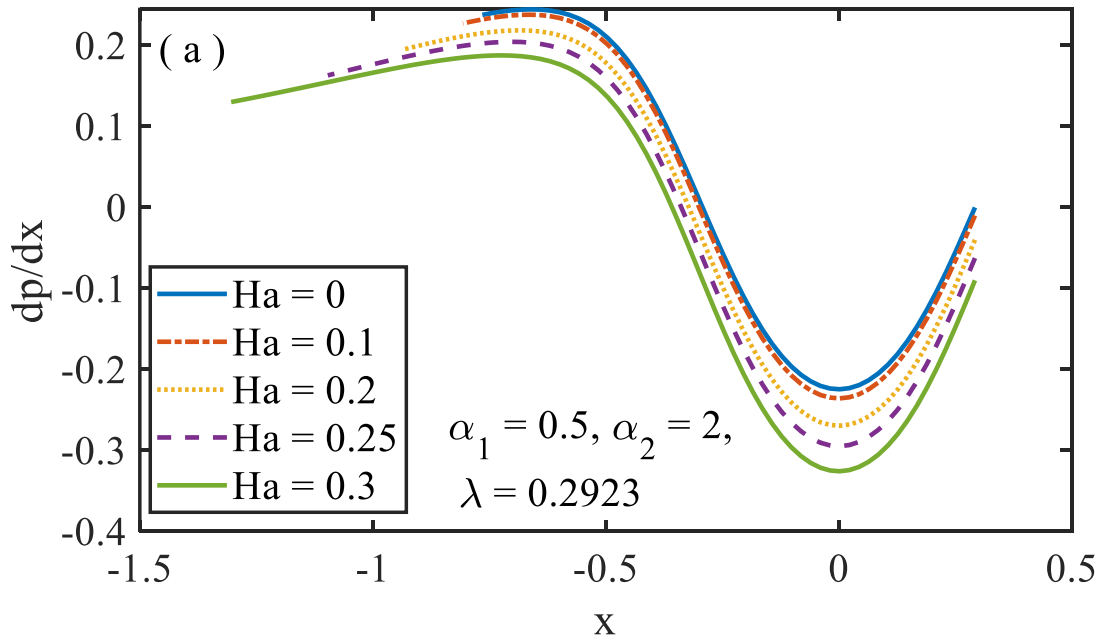

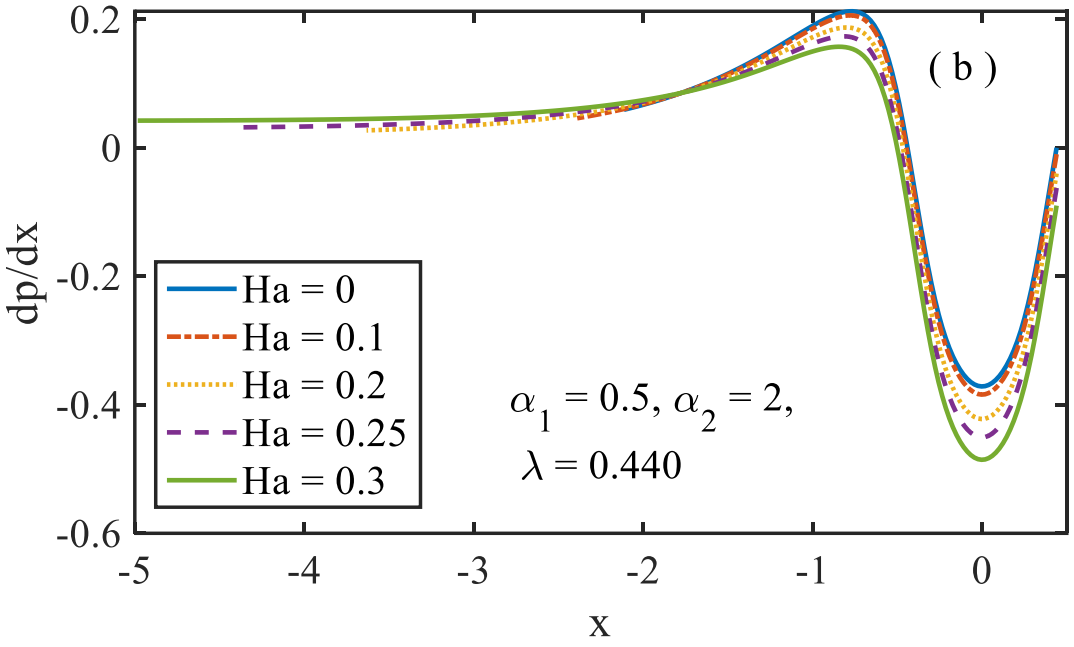

Fig. 9(a, b). Hartman number (*Ha*) effects on pressure gradient.

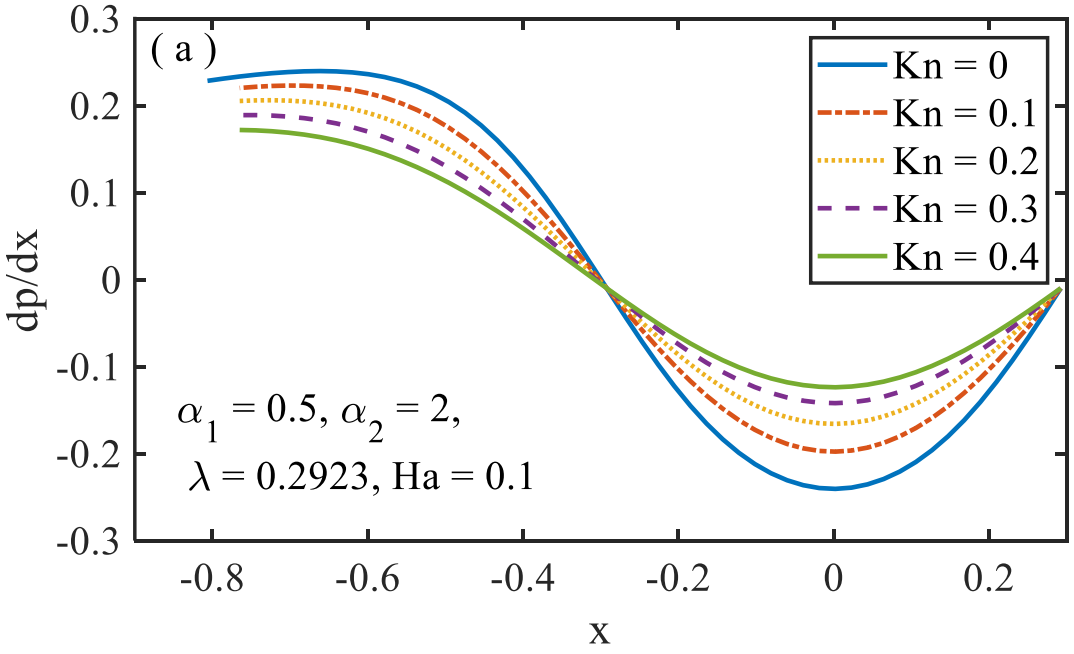

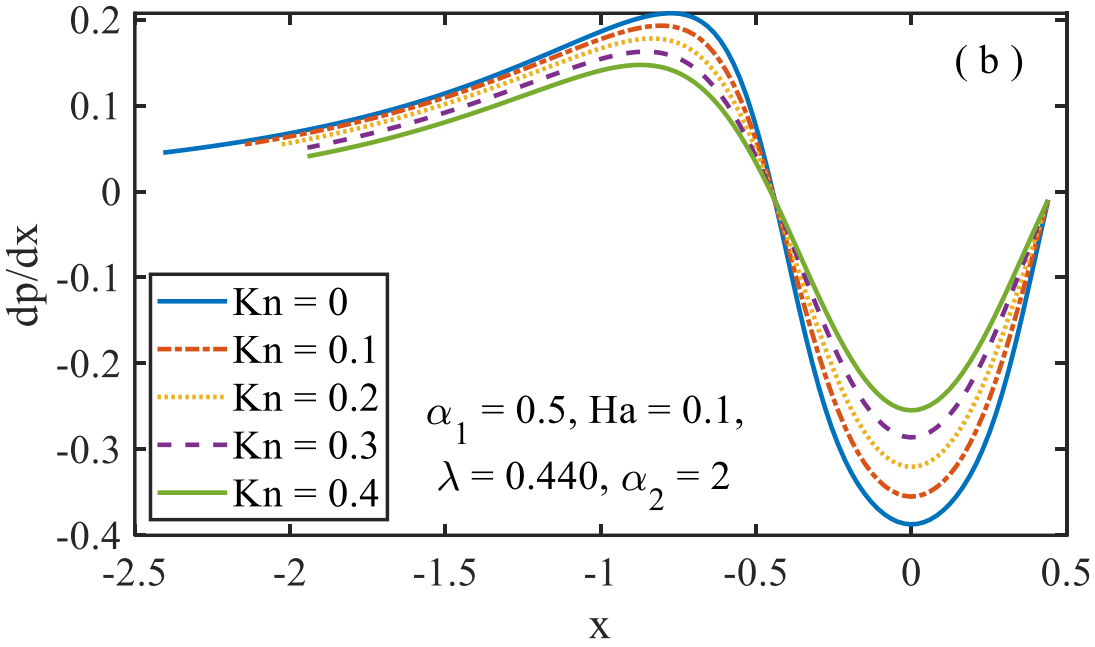
(b)
Kn = 0
Kn = 0.1
Kn = 0.2
Kn = 0.3
Kn = 0.4
α_1 = 0.5, Ha = 0.1,
λ = 0.440, α_2 = 2
dp/dx
x
0.2
0.1
0
-0.1
-0.2
-0.3
-0.4
-2.5
-2
-1.5
-1
-0.5
0
0.5

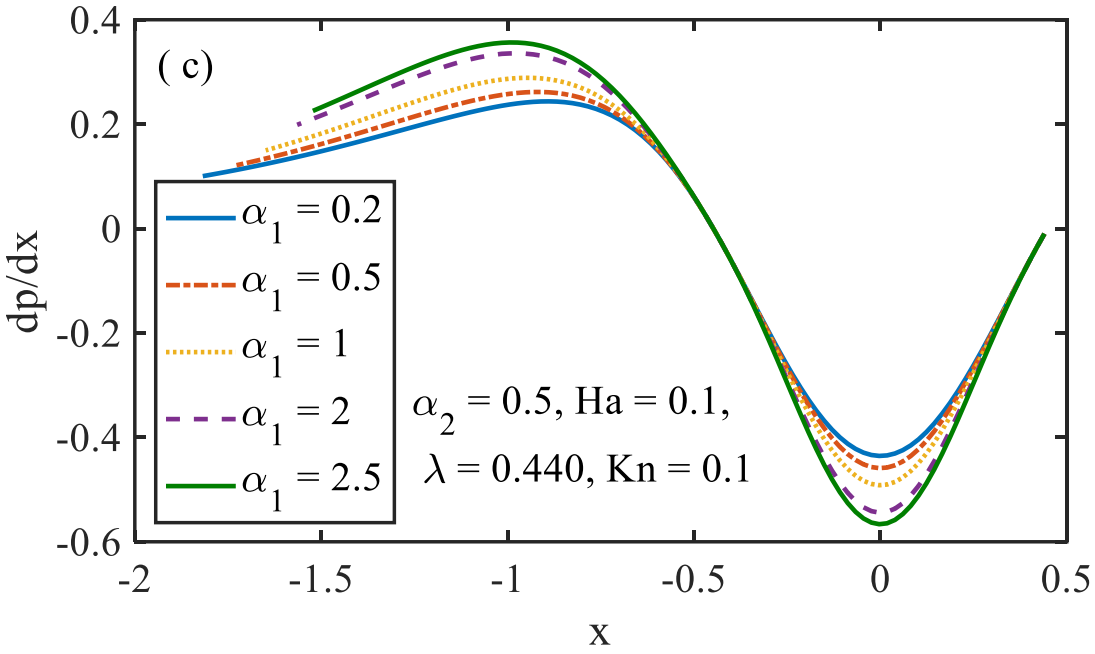
(c)
α_1 = 0.2
α_1 = 0.5
α_1 = 1
α_1 = 2
α_1 = 2.5
α_2 = 0.5, Ha = 0.1,
λ = 0.440, Kn = 0.1
dp/dx
x
0.4
0.2
0
-0.2
-0.4
-0.6
-2
-1.5
-1
-0.5
0
0.5

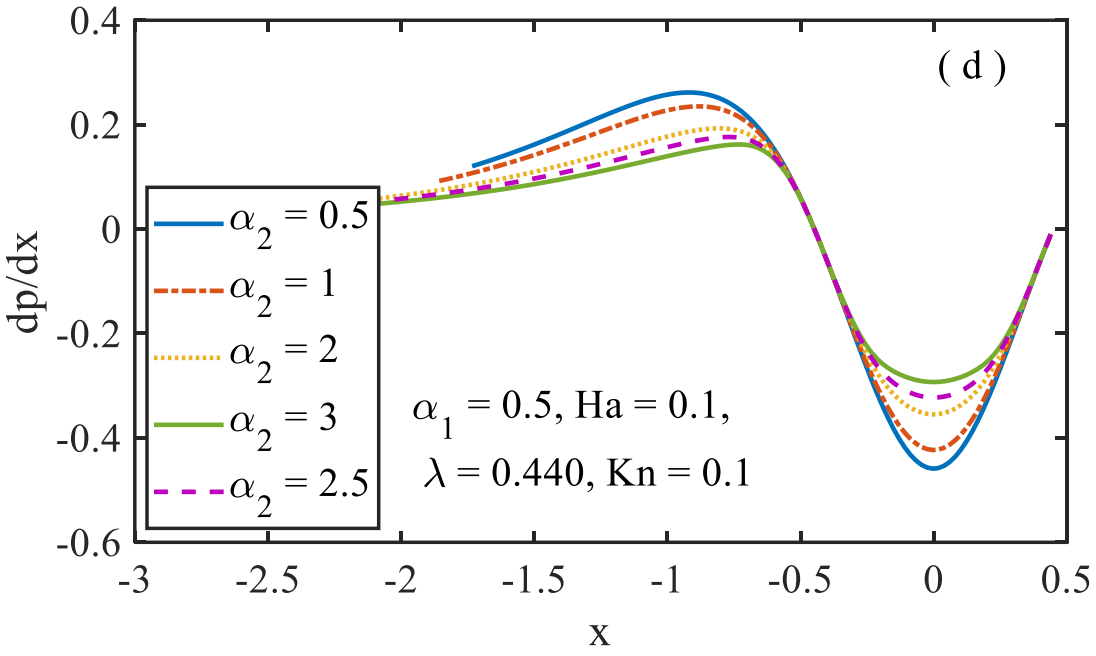

Fig. 10(a-d). Effects of slip parameter (*Kn*), α_1 and α_2 on pressure gradient.

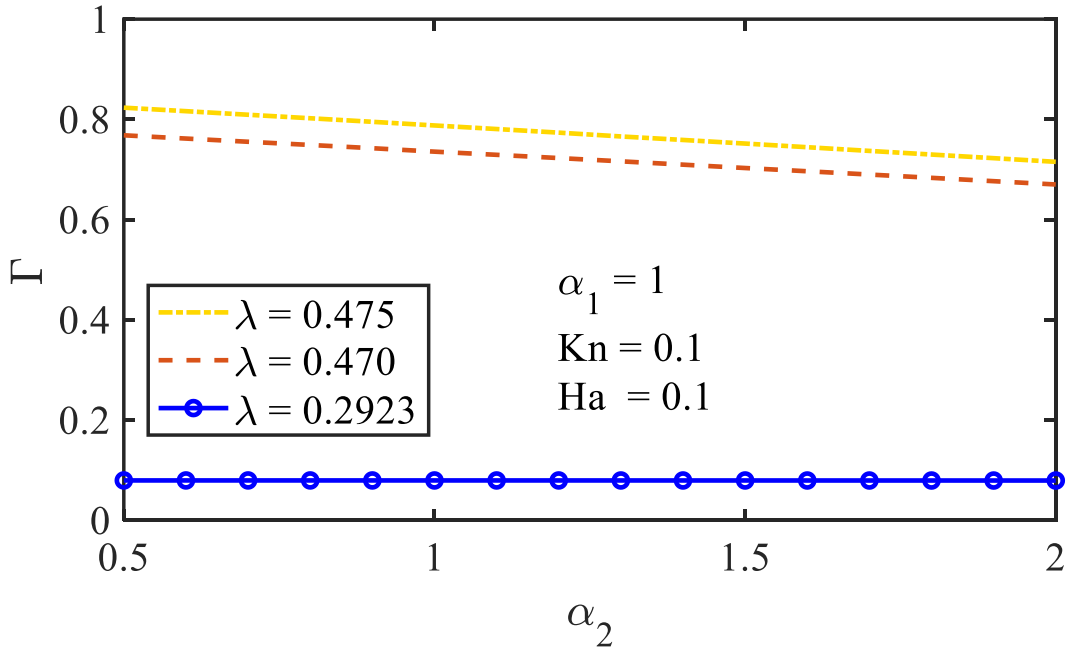

Fig. 11. Force function versus α_2.

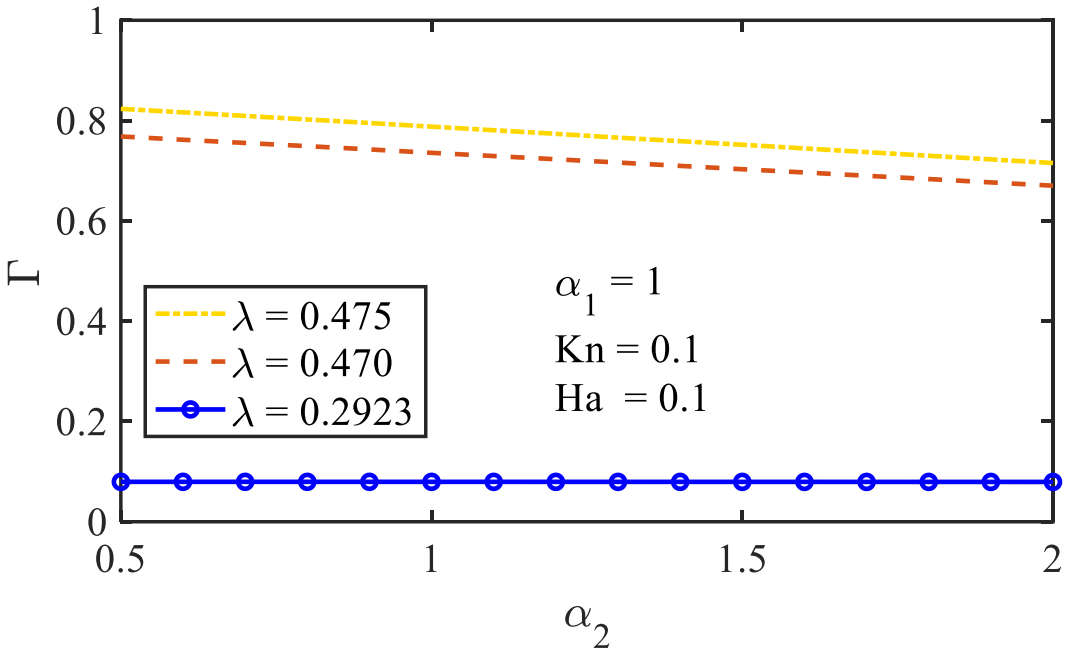

Fig. 12. Power function versus α_2.

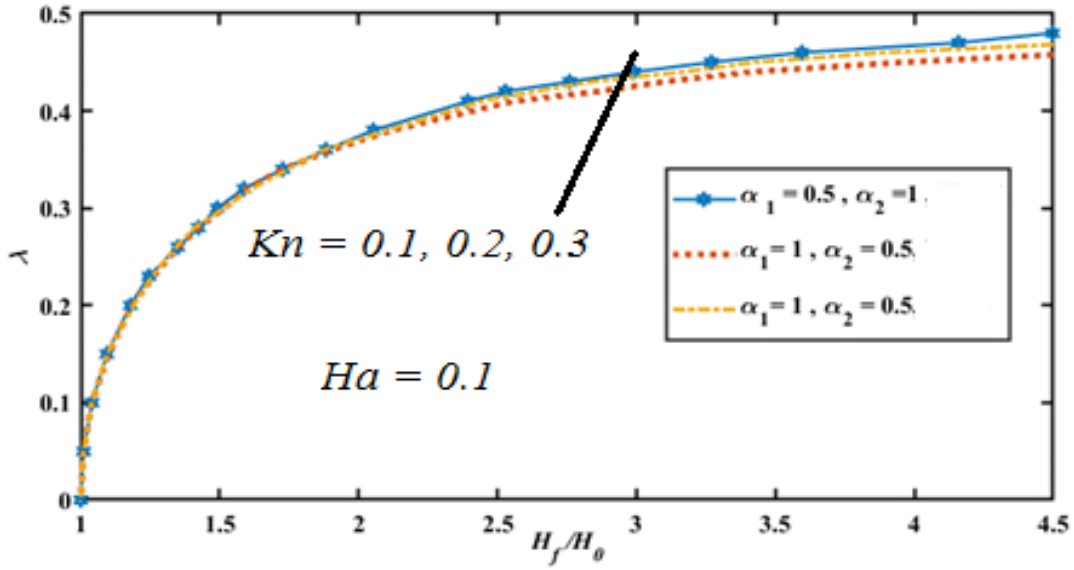

Fig. 13. Relationship between λ and H_f/H_0.